We are IntechOpen, the world's leading publisher of Open Access books Built by scientists, for scientists

6,900
Open access books available

185,000
International authors and editors

200M
Downloads

Our authors are among the

154
Countries delivered to

TOP 1%
most cited scientists

12.2%
Contributors from top 500 universities



WEB OF SCIENCE™

Selection of our books indexed in the Book Citation Index in Web of Science™ Core Collection (BKCI)

Interested in publishing with us?
Contact book.department@intechopen.com

Numbers displayed above are based on latest data collected.
For more information visit www.intechopen.com



Chapter 4

Pulse Density Modulation Applied to Series Resonant Inverter and Ac-Ac Conversion

Abdelhalim Sandali and Ahmed Chériti

Additional information is available at the end of the chapter

http://dx.doi.org/10.5772/intechopen.68324

Abstract

The PDM control joins together between the concepts of soft switching and hard switching. Its application to the series resonant inverter cancels the switching losses and uses dc bus without storage capacity. Objectively, the PDM controls led to ac-ac converters with high efficiency (zero switching loss), small size (no storage capacity) and with the possibility of a self power factor correction. However, the operating analysis of these converters is very complex because the operation is done on two time scales and leaves questions unanswered. The average modeling facilitates the analysis of the operation and leads to establish: (i) an analytical expression of the power factor, (ii) the linearity conditions of the power characteristic, and (iii) a model of ac-ac series resonant multi-converter which is independent of the carriers. In the case of ac-ac series resonant multi-converter, the coordination of carriers allows to shape the power characteristic. Among the three types of coordination presented, there is an original coordinate that linearizes the power characteristic. The results are validated by simulations carried out in Matlab SimPower systems.

Keywords: pulse density modulation, series resonant inverter, multi-inverter ac-ac converter, power factor correction, average modeling

1. Introduction

The soft-switching, appeared in the early eighties of last century, is a major event in the development of power electronics [1, 2]. Numerous research and conference sessions devoted to it reflect this importance. The soft switching is a conceptual breakthrough that led to technological advances. Indeed, to reduce the size of the reactive components, something that has a positive effect on the weight and size of converters, it is necessary to seek to increase the

INTECH
open science | open minds

© 2017 The Author(s). Licensee InTech. This chapter is distributed under the terms of the Creative Commons Attribution License (http://creativecommons.org/licenses/by/3.0), which permits unrestricted use, distribution, and reproduction in any medium, provided the original work is properly cited. CC BY

switching frequency. However, to increase the switching frequency of power semiconductor switches, it is imperative to create the conditions for reducing switching losses. Within the framework of soft switching concept, one considers that the most effective way to achieve this goal is to leave full-controlled power semiconductor devices to switch depending on their changing voltages and/or currents [3–5]. The power part of the converter plays an active role in determining the switching instants.

In resonant converters, implementing this concept, there is a shared determination of switching instants between the control part and power part of the converter: if a commutation is caused by the control, complementary commutation is caused by the voltage or current of the switch (ZVS or ZCS). The transmitted power control is done by the frequency modulation.

Pulse density modulation (PDM) control, appeared in the mid-1990s [6, 7], joins together the concept of soft switching and the traditional concept of hard switching by separating the roles of the control part and power part. The power part is responsible for determining the switching instants. The control part decides the nature of switching cycles (active or inactive). Its application to series resonance inverters has the major advantage to cancel the switching losses and to produce an output power factor near to unity [6–11]. The integration of these inverters in the ac-ac conversion makes it possible to save the smoothing filter and to have a sine-wave absorption at full power [6, 7]. Several recent researches are devoted to the development of PDM control and to the valorization of its applications [8–11]. The operating analysis presented in these papers focus on the output current. The input current (current drawn from the ac-supply) analysis is forsaken. This aspect constitutes the poor relation in the scientific literature dedicated to the PDM technique.

Fill this blank, clarify it why, and show how to exploit the benefits and manage the challenges are the objectives of this work. More than a synthesis of previous work, this chapter provides for the first time an average modeling of PDM inverters, an accurate determination of the linear operating conditions and an original linearization technique.

This chapter is organized as follows: in Section 3, we present the principle of PDM control and its integration in ac-ac converter. Section 4 is devoted to the description of a pulse density modulator. The conventional analysis is the subject of Section 5. The determinations of the input current of the ac-ac converter and its power factor in the case of single and multi-inverter configurations are presented. Section 6 is devoted to the average modeling of ac-ac series resonant converter in single- and multi-inverter configurations. Several cases of coordination of the carriers are discussed in Section 7. Simulation results are given in Section 8, and conclusion is presented in Section 9.

2. Principle

Pulse density modulation (PDM) is a type of control applied to the series resonance inverters. Turn-on and turn-off occur at zero crossings of the load current, because the switching frequency is taken equal to resonance frequency of the load. All commutations are lossless and without current gradient, and the input current of inverter is unidirectional. The inverter operation has the following improvements: (i) the switches are completely released from switching

stress; (ii) dc bus has no storage capacity; and (iii) reduction of electromagnetic noise. But, as the switching frequency is now fixed, it is impossible to use it to control the power.

To avoid this disadvantage, the control part generates a PDM pattern that determines whether a switching cycle is active or inactive. An active cycle is a normal operating cycle of the single-phase inverters. An inactive cycle is defined by the simultaneous state-on of same side switches (e.g., high side) and the simultaneous state-off of the other side switches (e.g., low side). It puts the output inverter in freewheel and, consequently, interrupts the flow of energy between input and output of the converter. The power control is now done by the PDM pattern duty cycle defined by:

$$d = n/k \tag{1}$$

with k is the number of total cycles per PDM pattern period (called PDM pattern length) and n=1, 2, …. or k.

The power control is thus done in a discrete manner with a resolution which depends on the length of the pattern.

Figure 1 shows the considered inverters and the transcription logic circuit of the PDM pattern in the gate control signals of the switches. We propose in **Figure 2** an operating model that clearly shows the coexistence of the two concepts (hard and soft switching). The PDM inverter is divided into soft inverter and hard buck. The transmitted power is controlled by the PDM pattern.

When the inverter is supplied by a single-phase diode bridge, the unit forms an ac-ac converter (LF to HF) (**Figure 3**). Since the input current of PDM inverter is unidirectional, it is possible to eliminate the smoothing filter (low frequency 2×50 or 2×60) and keep only a high frequency decoupling capacitor C_{HF}. The latter absorbs the high frequency ripple of the current in the

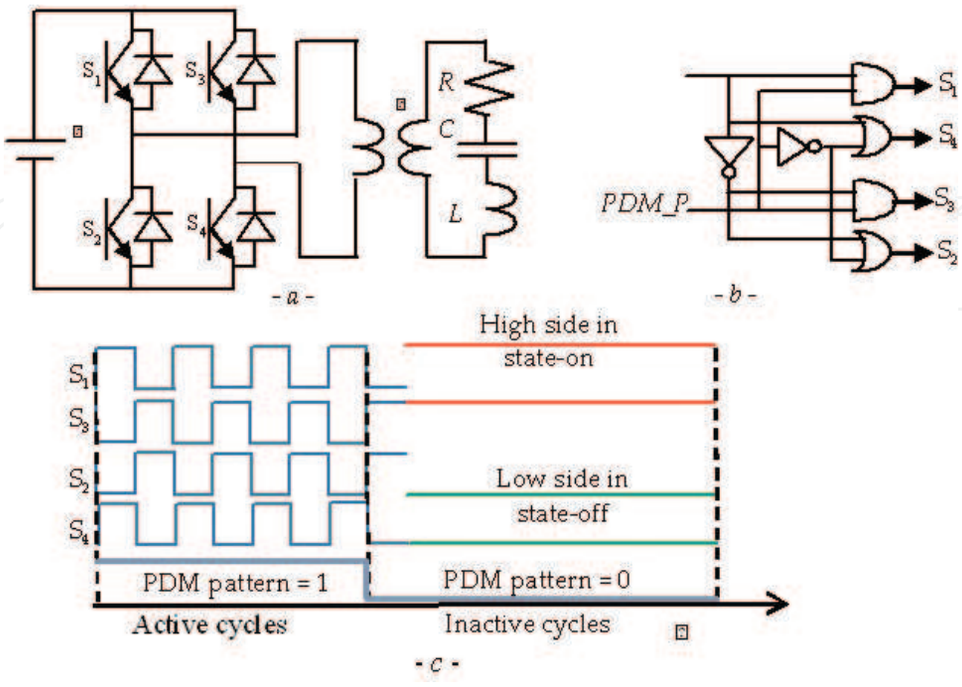


Figure 1. PDM inverter: topology, control and definition.

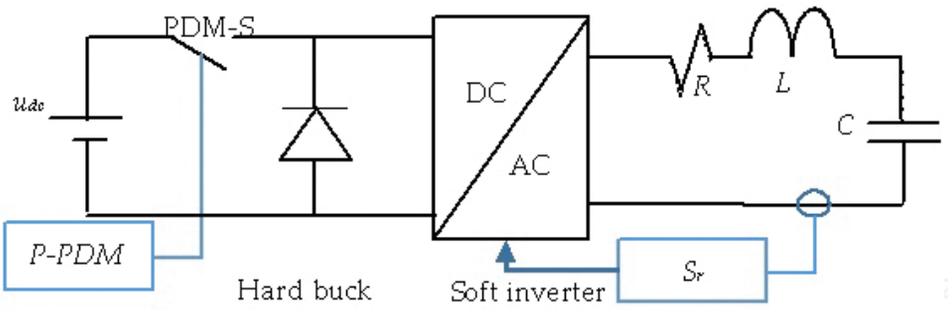


Figure 2. Decomposition of the PDM inverter in hard buck and soft inverter.

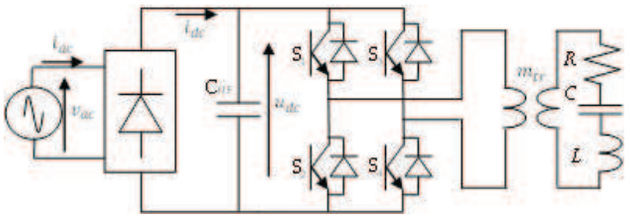


Figure 3. Ac-ac PDM converter (without smoothing filter).

rectifier. The result is a small-sized ac-ac converter because it is relieved of the smoothing filter). The current drawn by the ac-ac converter is a sinusoidal form, but is intersected by zero current phases when inactive cycles occur. In the following, we focus on the control, the transmitted power and the quality of current drawn by this ac-ac converter that will be called ac-ac PDM converter and noted PDMC.

3. PDM pattern generation

The PDM pattern generation is subject to two particular restrictions.

The first restriction concerns the adaptation of the PDM pattern frequency to the load resonance frequency. So that the switching cycles are not truncated, the PDM pattern period must be a multiple of the resonance period:

$$\text{First restriction } T_{PDM} = kT_r \text{ with } k \text{ is an integer} \tag{2}$$

To satisfy this restriction, several options are possible. We present below a PWM type technique but adapted to PDM control. It is based on a synchronous comparison of a control signal (e_c) and a triangular carrier (Car) [12]. The synchronous comparison is carried out by a conventional comparator followed by a D flip-flop (**Figure 4**).

When the PDM inverter is integrated into an ac-ac series resonant converter, it is necessary that the PDM pattern satisfies a second restriction: its period (frequency) must be a sub-multiple (multiple) of the period (frequency) of the dc link voltage:

http://dx.doi.org/10.5772/intechopen.68324

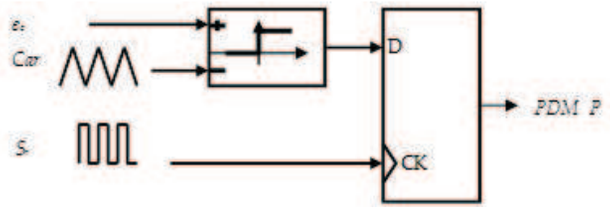


Figure 4. Adaptation of PDM frequency to resonance frequency by synchronous comparison.

$$\text{Second restriction } T_{dc} = qT_{PDM} \text{ with } q \text{ is an integer} \tag{3}$$

If this restriction is not satisfied, a continuous component can appear in the current drawn from the electrical network. The substitution of Eq. (2) into Eq. (3) leads to restriction:

$$T_{dc} = NT_{res} \text{ with } N = q * k \text{ is an integer} \tag{4}$$

To check this restriction, a calibration of the dc-voltage period seen by the inverter is performed by the definition of the ZCD signal (Zero Crossing Detector) [12]. This signal is determined by the synchronous comparison of the ac-supply voltage with positive and negative thresholds. The synchronous comparison is carried out here by the set two comparators—and logical gate—D flip-flop. ZCD is at the zero level during a time which is a multiple of the period of resonance and which can be very close to the period of the rectified voltage if the thresholds are close to zero. ZCD, when it's high, is used to reset the PDM pattern and the carrier's generator. Henceforth, the useful (or usable) period of the rectified voltage is automatically adjusted with a multiple of the resonance period, and the triangular carrier is synchronized to the latter. **Figure 5** shows the pattern generation circuit for an ac-ac PDM converter. The PDM pattern duty cycle is identified with the control signal because the carrier is triangular, whereas the carrier frequency represents the PDM pattern length. As a result, the control signal controls the power while the carrier frequency controls the power variation resolution. In the following section, we establish the relation between the control signal and the transmitted power and the impact of the carrier frequency on the quality of the current drawn from the ac-supply.

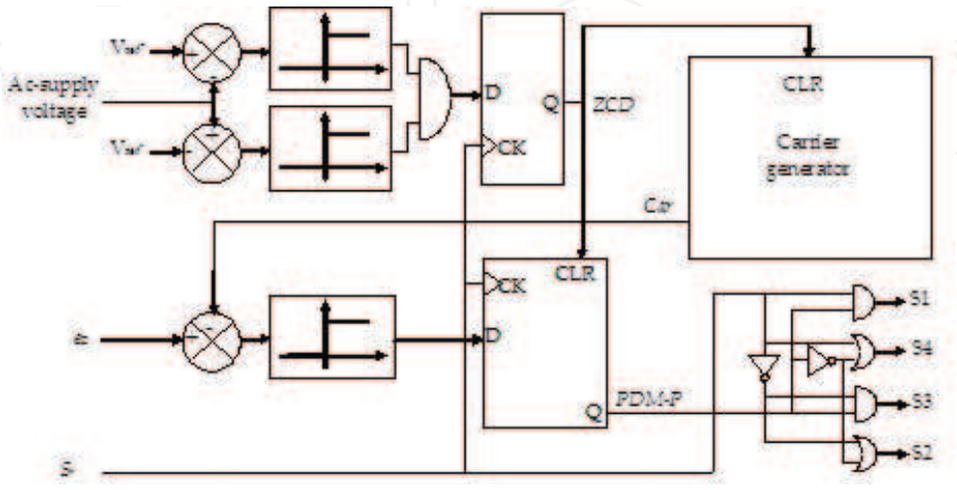


Figure 5. PDM pattern generator performing synchronous comparison and calibration.

4. Conventional analysis

4.1. Input current of ac-ac PDM converter

The drawn current from ac network and transmitted power by ac-ac series resonant converter are determined under the following assumptions: (i) the load has a low damping coefficient; (ii) C_{HF} capacitor absorbs HF component (twice the resonant frequency) of the inverter input current; (iii) the dc link voltage is assumed constant during a switching cycle; and (iv) no restriction is imposed on the PDM pattern except the restrictions of definition.

One determines successively the load current, the currents after and before the HF decoupling capacitor and the current drawn from the ac-supply. Then, one calculates the Fourier series of the latter current. In Ref. [12], it is shown that if the PDM pattern is generated according to the solution of Section3, the following results are obtained:

i. the transmitted power in pu varies linearly with the control signal:

$$p = e_c \tag{5}$$

ii. the spectrum of the drawn current consists of harmonic pairs spaced from $2qF_{\text{ac}}$

iii. and the power factor, calculated from the harmonic summation, is as follows:

$$PF = 1 \Big/ \sqrt{1 + \frac{2}{{e_c}^2} \sum_{h=1}^{\infty} \Big(sin\Big(\pi h(1 - e_c)\Big)/\pi h \Big)^2} \tag{6}$$

It is independent of the PDM pattern frequency. The power factor decreases continuously when the transmitted power in pu varies from 1 to 0.

Failing to improve the power-factor directly, an increase in the pattern frequency brings a better conditioning of the harmonic distortion (increase spacing and thus reject harmonics in high frequencies). But, it is observed that the more the frequency increases, the more one loses the linearity between power and control signal. We propose later in this chapter, a theoretical determination of the maximum frequency which preserves this linearity.

4.2. Input current of ac-ac multi-PDM converter and power factor correction

Correction by mutual compensation requires the use more than one inverter and an adapted control. The inverters are managed in such a way that the distortion produced by an inverter (zero current phase) is completely or partially masked by the other inverters. The inverters do not operate in inactive cycles simultaneously but successively. This management is based on the use of a set of interlaced carriers. This idea was developed for a system with several inverters and separate loads (each inverter feeds one load). Then, the idea was extended to the more realistic case of a single load [13]. The considered converter and its carriers are shown in **Figure 6**. It is called ac-ac multi-PDM converter and noted M-PDMC$_G$. If this converter consists of G inverters (Inv$_g$ with $g = 1, 2, \ldots, G$), the carrier associated with an Inv$_g$ is as follows:

http://dx.doi.org/10.5772/intechopen.68324

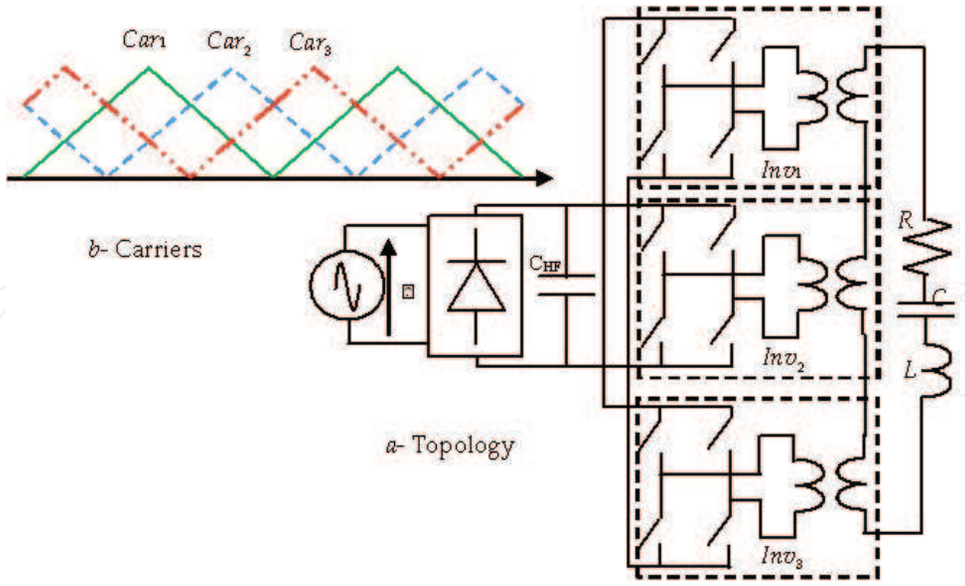


Figure 6. Ac-ac multi-PDM converter ($MPDMC_G$): topology and carriers in case $G=3$.

$$Car_g(\theta) = Car_1\left(\theta - (g-1)2\pi/G\right) \tag{7}$$

and all inverters have the same control signal:

$$e_{c,g} = e_c \tag{8}$$

This converter behavior is modeled by a bi-converter system with separate loads ($Conv_A$ and $Conv_B$) and variable parameters. The control signals, carriers and transformer ratios of $Conv_A$ and $Conv_B$ vary according to the control signal. **Figure 7** shows the topology of the bi-converter system and the control parameters. The results, detailed in Ref. [13], are as follows:

i. Power versus control signal is piecewise linear:

$$p = a_1 = g + (G.e_c - g)(2g-1) \tag{9}$$

Where $g - 1 = floor(G.e_c)$ (integer portion of $G.e_c$)

ii. the spectrum of the drawn current consists of harmonic pairs spaced from $2GqF_{ac}$

iii. the power factor, calculated from the harmonic summation, is:

$$PF = 1\Big/\sqrt{1 + 2(2g-1)^2\frac{\sum_{h=1}^{\infty}\left(sin(\pi hGe_c)/\pi h\right)^2}{\left(g^2 + (Ge_c - g)(2g-1)\right)^2}} \tag{10}$$

The power factor is equal to 1 in G points when the transmitted power is equal to $(j/G)^2$ 100% of its maximum value with $j = 1,\ 2,\ \ldots G$, and

iv. the maximum power is G^2 times greater than in the case of the PDMC.

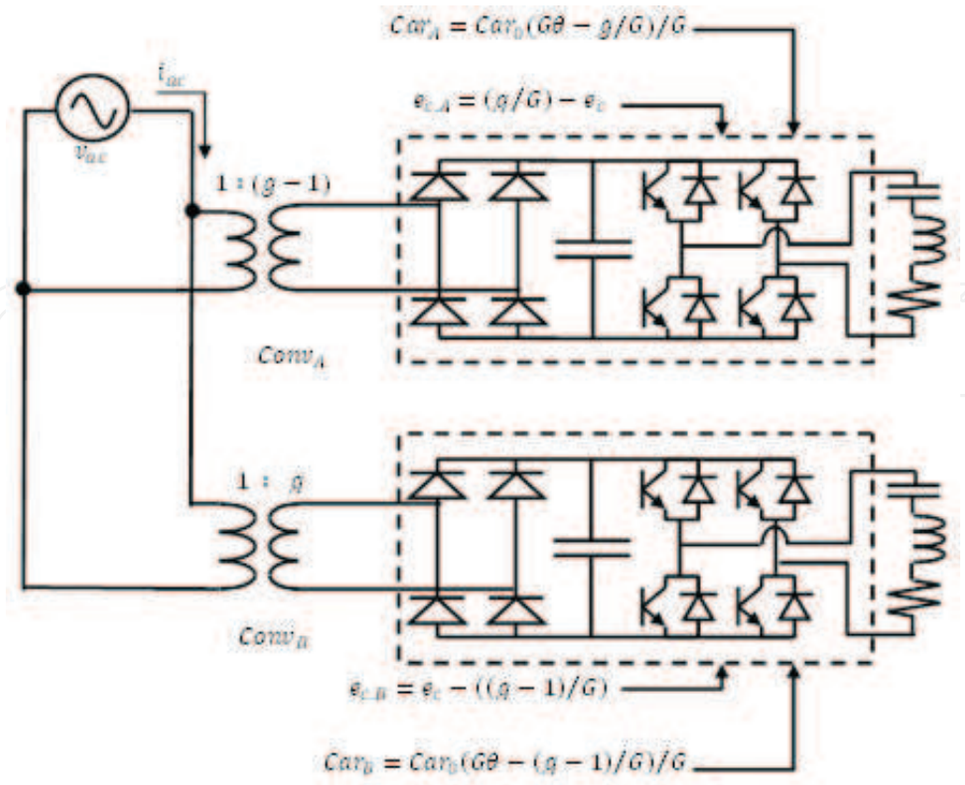


Figure 7. Bi-converter equivalent system when $(g-1)/G \leq e_c \leq g/G$.

This modeling is empirical because it is based solely on the observation of the converter behavior. However, since the behavior of a converter is defined by its topology and its control, the bi-converter model is only valid for the control law considered during the observation phase.

5. Analysis by average modeling

The average modeling is a powerful tool for the regulation and simulation of power electronics converters. Its main disadvantage is that it can predict only the mean value [14]. High frequency ripple is lost or predicted with inaccuracy [15]. In the case of PDM converters, the dc link between the rectifier and the inverter ensures high frequency decoupling. The rectifier's currents do not have high frequency ripple. The average modeling is thus a well-adapted tool for the determination of the low frequency side currents in the PDM converters. This technique is already applied successfully to the PDM-dual converters [16]. In the present work, it is applied for the first time to the PDM converters.

5.1. Average model of ac-ac PDM converter

5.1.1. Modeling of series resonant inverter

The time is subdivided into half-periods of resonance. Each half-period is indicated by an index n. The load voltage switches from $-u_{dc}$ to $+u_{dc}$ at instants $n(T_r/2)$ and from $+u_{dc}$ to $-u_{dc}$ at instants $(n+1)(T_r/2)$ with n even number. The capacitor voltage is as follows:

$$v_C(n+1) = -v_C(n)\ A + u_{dc} * (1+A) \text{ at the end of the } (n+1)\text{th half period} \tag{11}$$

$$v_C(n+2) = -v_C(n+1)\ A - u_{dc} * (1+A) \text{ at the end of the } (n+2)\text{th half period} \tag{12}$$

Under compact form, Eq. (11) and Eq. (12) become:

$$v_C(n) = -v_C(n-1)\ A + (-1)^{n+1} u_{dc} * (1+A) \text{ with } n \text{ even or odd} \tag{13}$$

Eq. (13) gives the value of the capacitor voltage at the end of the nth half-period as a function of the value taken at the $(n-1)$th half-period. According to the initial value, Eq. (13) becomes:

$$v_C(n) = (-1)^n \left\{ v_C(0)\ A^n - u_{dc} * (1+A) \sum_{i=0}^{n-1} A^i \right\} \tag{14}$$

Knowing that $\sum_{i=0}^{n-1} A^i = \frac{1-A^n}{1-A}$, Eq. (14) becomes :

$$v_C(n) = (-1)^n \left\{ v_C(0)\ A^n - u_{dc} * (1-A^n) \frac{1+A}{1-A} \right\} \tag{15}$$

The pic value of load current during the nth half-period is as follows:

$$\hat{i}(n) = \sqrt{C/L}\Big(v_C(n) - u_{dc}\Big) exp(\alpha T_r/4) \text{ for } n \text{ odd} \tag{16}$$

$$\hat{i}(n) = -\sqrt{C/L}\Big(v_C(n) + u_{dc}\Big) exp(\alpha T_r/4) \text{ for } n \text{ even} \tag{17}$$

During the nth half-period, the average value of inverter's input current is as follows:

$$\langle i \rangle(n) = \frac{2}{\pi} \hat{i}(n) = \frac{2}{\pi} \sqrt{C/L}\Big((-1)^{n+1} v_C(n) - u_{dc}\Big) \cdot exp(\alpha T_r/4) \tag{18}$$

Since the initial value of u_{dc} is zero, writing Eq. (18) for $n=0$ leads to:

$$\langle i \rangle(0) = -\frac{2}{\pi} \sqrt{C/L} v_C(0) \cdot exp(\alpha T_r/4) \tag{19}$$

It is deduced that

$$v_C(0) = -\frac{\pi}{2} \sqrt{C/L} \langle i \rangle(0) \cdot exp(-\alpha T_r/4) \tag{20}$$

The substitution of Eq. (20) into Eq. (15) yields:

$$v_C(n) = (-1)^n \left\{ -\frac{\pi}{2} \sqrt{C/L} exp(-\alpha T_r/4) \langle i \rangle(0)\ A^n - u_{dc} * (1-A^n) \frac{1+A}{1-A} \right\} \tag{21}$$

The substitution of Eq. (21) into Eq. (18) yields:

$$\langle i\rangle(n) = \langle i\rangle(0)\ A^n + u_{dc}\frac{4}{\pi}\sqrt{C/L}\frac{exp(-\alpha T_r/4)}{1-A}\left\{1 - A^n\frac{1+A}{2A}\right\} \tag{22}$$

Under the assumption:

$$(1+A)/2A \approx 1 \tag{23}$$

(this assumption is justified by the fact that $(\alpha T_r/2 = \pi\xi)$ is close to zero), expression (22) is identified with that of the current in $R_{eq} - L_{eq}$ series branch supplied by a voltage u_{dc} with:

$$R_{eq} = \frac{\pi}{4}\sqrt{\frac{L}{C}}\frac{1 - exp(-\alpha T_r/2)}{exp(-\alpha T_r/4)} \tag{24}$$

$$L_{eq} = \frac{R_{eq}}{\alpha} = L\frac{\pi}{4\xi}\frac{1 - exp(-\alpha T_r/2)}{exp(-\alpha T_r/4)} \tag{25}$$

The inverter dc side can then be modeled by the average circuit constituted by $R_{eq} - L_{eq}$ series branch.

5.1.2. Modeling of PDM inverter

Pulse density modulation is introduced by considering a fictitious hard buck that connects the voltage source to the inverter, represented by its average model. The unit constitutes the average model of PDM inverter (**Figure 8**). The current drawn by this converter is as follows:

$$i_{dc}(t) = \frac{u_{dc}}{R_{eq}}\left\{1 - \frac{1 - exp\Big(-(1-d)T_r/\tau_{eq}\Big)}{1 - exp(-T_r/\tau_{eq})}exp(-t/\tau_{eq})\right\} \text{ for } 0 \le t \le dT_{PDM} \tag{26}$$

$$i_{dc}(t) = 0 \text{ for } dT_{PDM} \langle t \le T_{PDM} \tag{27}$$

Using Eq. (26) and Eq. (27), the mean value, RMS value and form factor are calculated. We obtain:

$$\langle i\rangle_{dcT_{PDM}} = \frac{u_{dc}}{R_{eq}}\left\{d - \frac{\tau_{eq}}{T_{PDM}}\frac{\left(1 - exp\left(-d\frac{T_{PDM}}{\tau_{eq}}\right)\right)\left(1 - exp\left(-(1-d)\frac{T_{PDM}}{\tau_{eq}}\right)\right)}{\left(1 - exp\left(-\frac{T_{PDM}}{\tau_{eq}}\right)\right)}\right\} \tag{28}$$

$$\langle I_{dc}\rangle = \frac{u_{dc}}{R_{eq}}\sqrt{d - 2\frac{\tau_{eq}}{T_{PDM}}\frac{\left(1 - e^{-d\frac{T_{PDM}}{\tau_{eq}}}\right)\left(1 - e^{-(1-d)\frac{T_{PDM}}{\tau_{eq}}}\right)}{1 - e^{-\frac{T_{PDM}}{\tau_{eq}}}} + \frac{\tau_{eq}}{2\cdot T_{PDM}}\left(\frac{1 - e^{-(1-d)\frac{T_{PDM}}{\tau_{eq}}}}{1 - e^{-\frac{T_{PDM}}{\tau_{eq}}}}\right)^2\left(1 - e^{-2d\frac{T_{PDM}}{\tau_{eq}}}\right)} \tag{29}$$

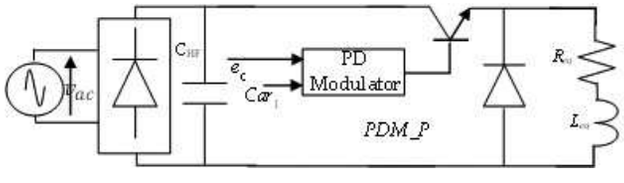


Figure 8. Average model of PDM inverter.

$$FF = \frac{d - \frac{\tau_{eq}}{T_{PDM}} \frac{\left(1-exp\left(-d\frac{T_{PDM}}{\tau_{eq}}\right)\right)\left(1-exp\left(-(1-d)\frac{T_{PDM}}{\tau_{eq}}\right)\right)}{1-exp\left(-\frac{T_{PDM}}{\tau_{eq}}\right)}}{\sqrt{d - 2\frac{\tau_{eq}}{T_{PDM}} \frac{\left(1-exp\left(-d\frac{T_{PDM}}{\tau_{eq}}\right)\right)\left(1-exp\left(-(1-d)\frac{T_{PDM}}{\tau_{eq}}\right)\right)}{1-exp\left(-\frac{T_{PDM}}{\tau_{eq}}\right)} + \frac{\tau_{eq}}{2 \cdot T_{PDM}} \left(\frac{1-exp\left(-(1-d)\frac{T_{PDM}}{\tau_{eq}}\right)}{1-exp\left(-\frac{T_{PDM}}{\tau_{eq}}\right)}\right)^2 \left(1 - exp\left(-2d\frac{T_{PDM}}{\tau_{eq}}\right)\right)}} \tag{30}$$

5.1.3. Extension to ac-ac converter

Now, we consider that the voltage u_{dc} is supplied by a single-phase diode rectifier. During the jth PDM pattern period, we suppose that this voltage is as follows:

$$u_{dc}(j) = \hat{V}_{ac} sin(\theta_j) \tag{31}$$

with $\theta_j = \frac{\pi}{q}\frac{2j-1}{2}$ is the midpoint of jth pattern period.

By substitution of Eq. (31) into Eqs. (28) and (29), we obtain mean value, RMS value and form factor of i_{dc} during jth pattern period:

$$\langle i_{dc} \rangle_{T_{PDM}} = \frac{\hat{V}_{ac}}{R_{eq}} \left\{ d - \frac{\tau_{eq}}{T_{PDM}} \frac{\left(1 - exp\left(-d\frac{T_{PDM}}{\tau_{eq}}\right)\right)\left(1 - exp\left(-(1-d)\frac{T_{PDM}}{\tau_{eq}}\right)\right)}{1 - exp\left(-\frac{T_{PDM}}{\tau_{eq}}\right)} \right\} sin(\theta_j) \tag{32}$$

$$I_{dc} = \frac{\hat{V}_{ac}}{R_{eq}} \sqrt{d - \frac{2\tau_{eq}}{T_{PDM}} \frac{1 - e^{-(1-d)\frac{T_{PDM}}{\tau_{eq}}}}{1 - e^{-\frac{T_{PDM}}{\tau_{eq}}}} \left\{ 1 - e^{-d\frac{T_{PDM}}{\tau_{eq}}} + \frac{1}{4} \left(\frac{1 - e^{-(1-d)\frac{T_{PDM}}{\tau_{eq}}}}{1 - e^{-\frac{T_{PDM}}{\tau_{eq}}}} \right) \left(1 - e^{-2d\frac{T_{PDM}}{\tau_{eq}}} \right) \right\}} sin(\theta_j) \tag{33}$$

In the appendix, we show that the fundamental component and the RMS value of the current drawn from ac-supply (Rectifier input current) and the mean and RMS values of the inverter input current during the jth PDM pattern period are linked by the following relationships:

$$\frac{\hat{I}_f}{(\hat{V}_{ac}/R_{eq})} = \frac{\langle i_{dc} \rangle_{T_{PDM}}(j)}{(\hat{V}_{ac}/R_{eq}) sin(\theta_j)} \tag{34}$$

$$\frac{I_{ac}}{(\hat{V}_{ac}/R_{eq})} = \frac{I_{dc}(j)}{(\hat{V}_{ac}/R_{eq}) sin(\theta_j)} \frac{1}{\sqrt{2}} \tag{35}$$

Knowing that in the case of a single-phase diode rectifier, the displacement factor is unitary, and the power factor is assimilated to the distortion factor:

$$PF = \frac{\hat{I}_f}{\sqrt{2} \cdot I_{ac}} \tag{36}$$

Substitution of Eqs. (35), (34), (33) and (32) into Eq. (36) yields:

$$PF = \frac{e_c - q2F_{ac}\tau_{eq}\dfrac{\left(1-exp(-\,e_c/q2F_{ac}\tau_{eq})\right)\left(1-exp\left(-(1-e_c)/q2F_{ac}\tau_{eq}\right)\right)}{1-exp(-\,1/q2F_{ac}\tau_{eq})}}{\sqrt{e_c - q4F_{ac}\tau_{eq}\dfrac{\left(1-exp\left(-\frac{e_c}{q2F_{ac}\tau_{eq}}\right)\right)\left(1-exp\left(-\frac{(1-e_c)}{q2F_{ac}\tau_{eq}}\right)\right)}{1-exp\left(-\frac{1}{q2F_{ac}\tau_{eq}}\right)} + qF_{ac}\tau_{eq}\left(\dfrac{1-e^{-\frac{(1-e_c)}{q2F_{ac}\tau_{eq}}}}{1-e^{-\frac{1}{q2F_{ac}\tau_{eq}}}}\right)^2\left(1-e^{-2\frac{e_c}{q2F_{ac}\tau_{eq}}}\right)}} \tag{37}$$

The transmitted power is defined by:

$$P = \frac{1}{2}\hat{V}_{ac}\hat{I}_f \tag{38}$$

Substitution of Eqs. (32) and (34) into Eq. (38) gives the transmitted power in pu:

$$p = e_c - q2F_{ac}\tau_{eq}\frac{\left(1-exp(-\,e_c/q2F_{ac}\tau_{eq})\right)\left(1-exp\left(-\,(1-e_c)/q2F_{ac}\tau_{eq}\right)\right)}{1-exp(-\,1/q2F_{ac}\tau_{eq})} \tag{39}$$

Its reference is as follows:

$$P_{ref} = \frac{1}{2}\hat{V}_{ac}{}^2/R_{eq} \tag{40}$$

The expressions (37) and (39) can be greatly simplified, if we consider the hypothesis:

$$\text{H1} : q2F_{ac}\tau_{eq} \ll 1 \tag{41}$$

They become:

$$PF \approx \sqrt{e_c} \tag{42}$$

$$p \approx e_c \tag{43}$$

To establish the maximum value that $q2F_{ac}\tau_{eq}$ can take without the approximations becoming imprecise, we calculate the relative errors in the most unfavorable case:

$$\frac{\Delta PF}{PF} = \frac{|PF(e_c) - \sqrt{e_c}|}{PF(e_c)} \tag{44}$$

$$\frac{\Delta p}{p} = \frac{|p(e_c) - e_c|}{p(e_c)} \tag{45}$$

It is checked that the most unfavorable case, that is, the errors are maximal, occurs when e_c is minimal. For different values of $\boldsymbol{e_{c,\,min}}$, we plot these errors versus $\boldsymbol{q2F_{ac}\tau_{eq}}$ (**Figure 9**). It is noted that the power error is not limited (it increase continuously). Eq. (43) gives values that can be truly erroneous if $\boldsymbol{q2F_{ac}\tau_{eq}}$ is not kept below a maximum value $(\boldsymbol{q2F_{ac}\tau_{eq}})_{max}$. This means that in order to maintain a relative error less than a given limit, when $\boldsymbol{ec}$ varies between 1 and $\boldsymbol{e_{c,\,min}}$, the coefficient q must respect the constraint:

http://dx.doi.org/10.5772/intechopen.68324

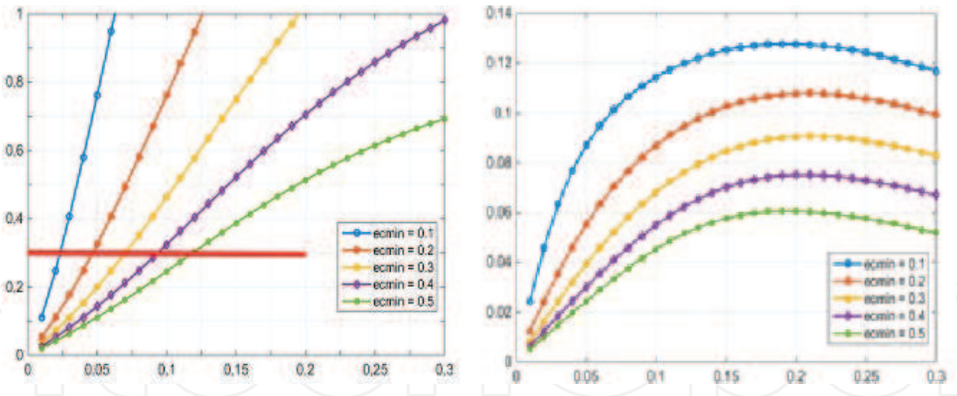


Figure 9. Power and power factor errors versus $q2F_{ac}\tau_{eq}$.

$$q \le q_{max} = (q2F_{ac}\tau_{eq})_{max}/2F_{ac}\tau_{eq} \tag{46}$$

This constraint means that:

$$F_{car}\tau_{eq} \le (q2F_{ac}\tau_{eq})_{max} \tag{47}$$

because

$$q=(F_{PDM}=F_{car})/2F_{ac} \tag{48}$$

In **Figure 9**, we can directly read $(q2F_{ac}\tau_{eq})_{max}$ as a function of the maximum permissible error and for different values of $e_{c,min}$. If, for example, to maintain the error below 30%, the carrier frequency must be less than the maximum frequency:

$$F_{car} \le (F_{car})_{max}=0.023/\tau_{eq} \text{ si } e_{c,min}=0.1 \tag{49}$$

$$F_{car} \le (F_{car})_{max}=0.119/\tau_{eq} \text{ si } e_{c,min}=0.5 \tag{50}$$

Eqs. (49) and (50) can be put in the general form:

$$F_{car}\tau_{eq} \le \mathcal{L}_x(e_{c,min}) \tag{51}$$

where $\mathcal{L}_x(e_{c,min})$ is the maximum value that $F_{car}\tau_{eq}$ must not exceed if we want Eq. (43) to give the power with a tolerance less than x when e_c varies from 1 to $e_{c,min}$.

Eq. (26) shows that i_{dc} has a static component and a transient component:

$$i_{dc}{}^{s}(t) = \frac{u_{dc}}{R_{eq}} \text{ for } 0 \le t \le (dT_{PDM} = e_c/F_{car}) \tag{52}$$

$$i_{dc}{}^{t}(t) = \frac{u_{dc}}{R_{eq}} \frac{1 - exp\left(-(1-d)T_r/\tau_{eq}\right)}{1 - exp(-T_r/\tau_{eq})} exp(-t/\tau_{eq}) \text{ for } 0 \le t \le (dT_{PDM} = e_c/F_{car}) \tag{53}$$

Eq. (53) shows that the more we reduce $\mathcal{L}_x(e_{c,min})$, the more transient component is damped. Consequently, the currents become:

$$i_{dc}(t) = \frac{u_{dc}}{R_{eq}} * PDM_P \tag{54}$$

$$i_{ac}(t) = \frac{u_{ac}}{R_{eq}} * PDM_P \tag{55}$$

If the power and the power factor are determined from Eqs. (54) and (55), we find the expressions (42) and (43). This proves that the hypothesis H1, which allowed the passage of Eqs. (37) and (39) to Eqs. (42) and (43), indirectly signifies the predominance of the static component in i_{dc}.

5.2. Average model of ac-ac Multi-PDM converter (MPDMC)

The converter considered is that shown in **Figure 6**. By replacing each inverter by its average model, one builds the MPDMC's average model (**Figure 10**).

According to this average model, the current drawn by the gth inverter is as follows:

- zero, if its pattern is at zero:

$$i_{ac,g} = 0 \; if \; PDM_P_g = 0 \tag{56}$$

- identical to the current drawn by a PDMC if its pattern is at 1, and the patterns of all the other inverters are at zero:

$$i_{ac,g} = i_{ac} \text{ if } PDM_P_g = 1 \text{ and } PDM_P_{j \neq g} = 0 \tag{57}$$

- identical to the current drawn by a PDMC multiplied by the number of inverters whose patterns are at 1, if its pattern is at 1:

$$i_{ac,g} = i_{ac} \sum_{j=1}^{G} PDM_P_j \tag{58}$$

Eqs. (56), (57) and (58) can be written in the form:

$$i_{ac,g} = i_{ac} PDM_P_g \sum_{j=1}^{G} PDM_P_j \tag{59}$$

The current drawn by the MPDMC is the sum of the currents drawn by the various inverters:

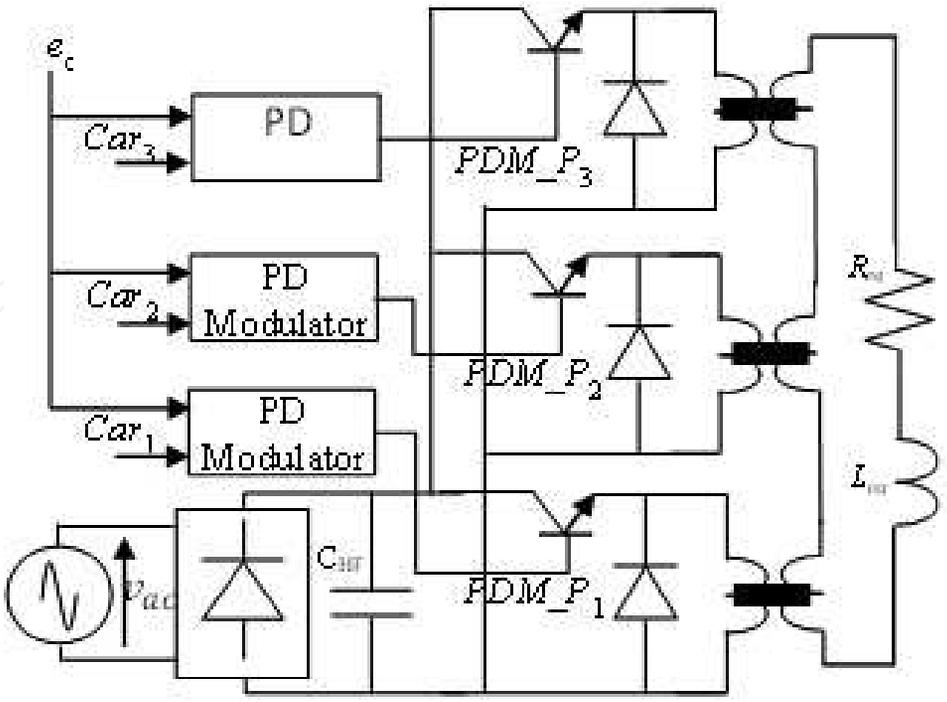


Figure 10. Average model of MPDMC.

$$i_{ac,MPDMC} = \sum_{g=1}^{G} i_{ac,g} \tag{60}$$

Substitution of Eqs. (59) and (60) into Eq. (55) yields:

$$i_{ac,MPDMC} = \frac{v_{ac}}{R_{eq}} \left(\sum_{g=1}^{G} PDM_P_g \right)^2 \tag{61}$$

Comparing between Eqs. (61) and (55), we see that a M-PDMC is a PDMC that would be modulated by the square of the sum of the different patterns.

6. MPDMC features: power factor correction and transmitted power

The behavior of the MPDMC is determined by three elements: the control signal, the carrier and the coordination of all the carriers. In this section, we discuss three types of coordination.

6.1. First coordination: interlaced carriers

In **Figures 11** and **12**, we traced interlaced carriers, the patterns PDM_P_g and $\left(\sum_{g=1}^{G} PDM_P_g\right)^2$ in the cases $G=2$ and $G=3$.

In the case $G=3$, when $0 \le e_c \le 1/3$, we have 1 or 0 pattern at 1:

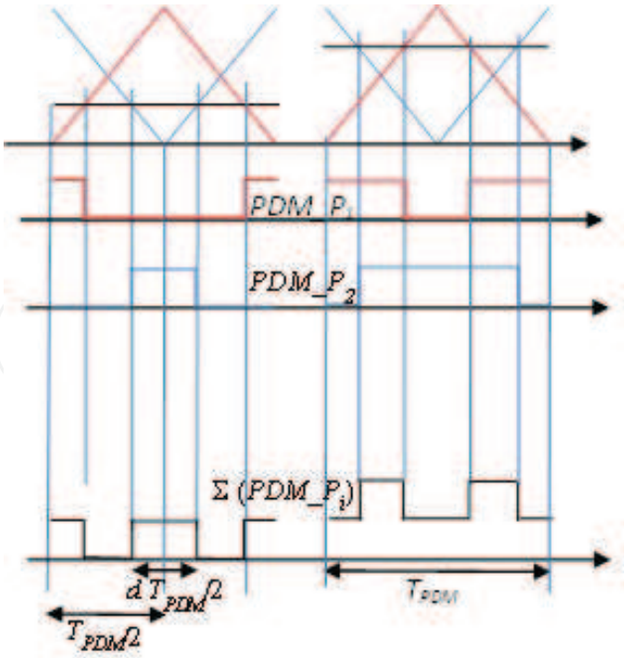


Figure 11. Interlaced carriers for $MPDMC_2$.

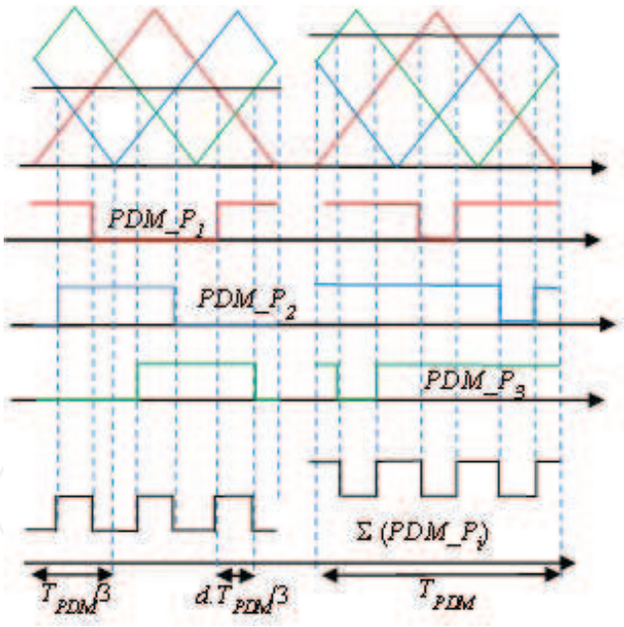


Figure 12. Interlaced carriers for $MPDMC_3$.

$$\left(\sum_{g=1}^{G} PDM_P_g\right)^2 = 1 \text{ during } d(T_{PDM}/3) \tag{62.1.1}$$

$$\left(\sum_{g=1}^{G} PDM_P_g\right)^2 = 0 \text{ during } (1-d)(T_{PDM}/3) \tag{62.1.2}$$

$$\text{with } d = 3.e_C \tag{62.1.3}$$

when $1/3 \le e_c \le 2/3$, we have 2 or 1 patterns at 1 :

$$\left(\sum_{g=1}^{G} PDM_P_g\right)^2 = 2^2 \text{ during } d(T_{PDM}/3) \tag{62.2.1}$$

$$\left(\sum_{g=1}^{G} PDM_P_g\right)^2 = 1^2 \text{ during } (1-d)(T_{PDM}/3) \tag{62.2.2}$$

$$\text{with } d = 3.e_C - 1 \tag{62.2.3}$$

when $2/3 \le e_c \le 3/3$, we have 3 or 2 patterns at 1 :

$$\left(\sum_{g=1}^{G} PDM_P_g\right)^2 = 3^2 \text{ during } d(T_{PDM}/3) \tag{62.3.1}$$

$$\left(\sum_{g=1}^{G} PDM_P_g\right)^2 = 2^2 \text{ during } (1-d)(T_{PDM}/3) \tag{62.3.2}$$

$$\text{with } d = 3.e_C - 2 \tag{62.3.3}$$

Eqs. (62) can be generalized as follows:

when $(g-1)/G \le e_c \le g/G$, we have g or $g-1$ patterns at 1 :

$$\left(\sum_{g=1}^{G} PDM_P_g\right)^2 = g^2 \text{ during } d(T_{PDM}/G) \tag{63.1}$$

$$\left(\sum_{g=1}^{G} PDM_P_g\right)^2 = (g-1)^2 \text{ during } (1-d)(T_{PDM}/G) \tag{63.2}$$

$$\text{with } d = G.e_C - (g-1) \tag{63.3}$$

$$\text{where } (g-1) = floor(G.e_C) \tag{63.4}$$

From Eq. (63), we determine average value and RMS value of $\left(\sum_{g=1}^{G} PDM_P_g\right)^2$:

$$\left\langle \left(\sum_{g=1}^{G} PDM_P_g\right)^2 \right\rangle = g^2 d + (g-1)^2(1-d) \tag{64}$$

$$RMS\left(\left(\sum_{g=1}^{G} PDM_P_g\right)^2\right) = \sqrt{g^4 d + (g-1)^4(1-d)} \tag{65}$$

Using Eqs. (64) and (65), we determine transmitted power and power factor :

$$p = \left\langle \left(\sum_{g=1}^{G} PDM_P_g \right)^2 \right\rangle = g^2 d + (g-1)^2 (1-d) \tag{66}$$

$$PF = \left\langle \left(\sum_{g=1}^{G} PDM_P_g \right)^2 \right\rangle \Big/ RMS\left(\left(\sum_{g=1}^{G} PDM_P_g \right)^2 \right) = \frac{1 + \left(\left(g/(g-1) \right)^2 - 1 \right) d}{\sqrt{1 + \left(\left(g/(g-1) \right)^4 - 1 \right) d}} \tag{67}$$

$$\text{with } d = G.e_C - (g-1) \tag{68}$$

$$\text{and } (g-1) = floor(G.e_C) \tag{69}$$

We find: (i) the same characteristic power versus control signal as in Section 5 and (ii) the power factor is determined by an analytic expression and not by a summation of the harmonics.

6.2. Second coordination: distribution in uniform bandwidths

Instead of reducing the total harmonic distortion by a mutual compensation of the individual distortions (produced by each inverter), one can reduce it differently: all inverters operate at full power or at standstill, and they do not produce distortion, except one that operates in modulation to ensure power variation. To achieve this correction, the carriers are distributed in uniform bandwidths. All carriers have the same peak value:

$$\widehat{Car}_g = 1/G \tag{70}$$

In **Figures 13** and **14**, we plot uniformly superimposed carriers, associated patterns PDM_P_g and $\left(\sum_{g=1}^{G} PDM_P_g \right)^2$ in the cases $G=2$ and $G=3$.

In the case $G=3$, Eq. (70) leads to:

$$\widehat{Car}_1 = \widehat{Car}_2 = \widehat{Car}_3 = 1/3 \tag{71}$$

when $0 \le e_c \le 1/3$, we have 1 or 0 pattern at 1:

$$\left(\sum_{g=1}^{G} PDM_P_g \right)^2 = 1 \text{ during } d.T_{PDM} \tag{72.1.1}$$

$$\left(\sum_{g=1}^{G} PDM_P_g \right)^2 = 0 \text{ during } (1-d).T_{PDM} \tag{72.1.2}$$

$$\text{with } d = e_C / \widehat{Car}_1 = 3.e_C \tag{72.1.3}$$

when $1/3 \le e_c \le 2/3$, we have 2 or 1 patterns at 1:

http://dx.doi.org/10.5772/intechopen.68324

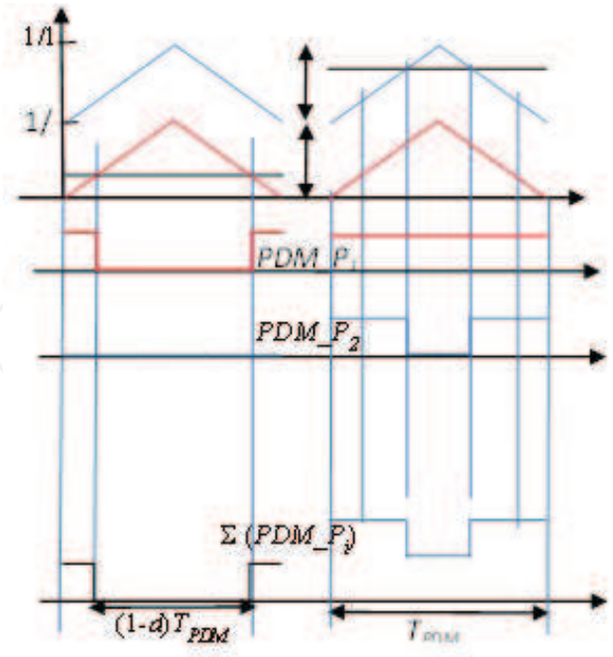


Figure 13. Carriers distributed in uniform bandwidths, $G=2$.

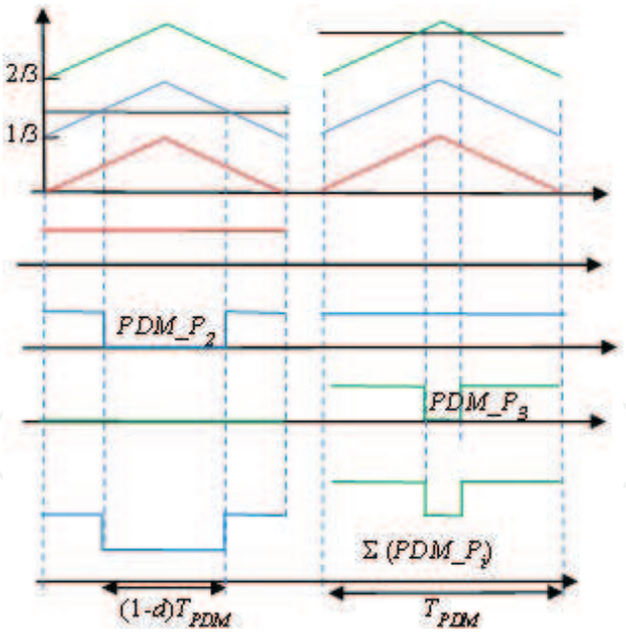


Figure 14. Carriers distributed in uniform bandwidths, $G=3$.

$$\left(\sum_{g=1}^{G} PDM_P_g\right)^2 = 2^2 \text{ during } d.T_{PDM} \tag{72.2.1}$$

$$\left(\sum_{g=1}^{G} PDM_P_g\right)^2 = 1^2 \text{ during } (1-d).T_{PDM} \tag{72.2.2}$$

$$\text{with } d = (e_C - 1/3)/\widehat{Car}_2 = 3.e_C - 1 \tag{72.2.3}$$

when $2/3 \le e_c \le 3/3$, we have 3 or 2 patterns at 1:

$$\left(\sum_{g=1}^{G} PDM_P_g\right)^2 = 3^2 \text{ during } d.T_{PDM} \tag{72.3.1}$$

$$\left(\sum_{g=1}^{G} PDM_P_g\right)^2 = 2^2 \text{ during } (1-d).T_{PDM} \tag{72.3.2}$$

$$\text{with } d = (e_C - 2/3)/\widehat{Car}_3 = 3.e_C - 2 \tag{72.3.3}$$

Eqs. (72) can be generalized as follows:

when $(g-1)/G \le e_c \le g/G$, we have g or $g-1$ patterns at 1:

$$\left(\sum_{g=1}^{G} PDM_P_g\right)^2 = g^2 \text{ during } \ d.T_{PDM} \tag{73.1}$$

$$\left(\sum_{g=1}^{G} PDM_P_g\right)^2 = (g-1)^2 \text{ during } (1-d).T_{PDM} \tag{73.2}$$

$$\text{with } d = \Big(G.e_C - (g-1)\Big)/(G.\widehat{Car}_g) \tag{73.3}$$

$$where\ (g-1) = floor(G.e_C) \tag{73.4}$$

Using Eq. (73), we determine transmitted power and power factor:

$$p = \left\langle \left(\sum_{g=1}^{G} PDM_P_g\right) \right\rangle^2 = g^2 d + (g-1)^2(1-d) \tag{74}$$

$$PF = \left\langle \left(\sum_{g=1}^{G} PDM_P_g\right) \right\rangle^2 \Big/ RMS\left(\left(\sum_{g=1}^{G} PDM_P_g\right)^2\right) = \frac{1 + \Big(\Big(g/(g-1)\Big)^2 - 1\Big)d}{\sqrt{1 + \Big(\Big(g/(g-1)\Big)^4 - 1\Big)d}} \tag{75}$$

$$\text{with } d = \Big(G.e_C - (g-1)\Big)/(G.\widehat{Car}_g) = G.e_C - (g-1) \tag{76}$$

$$\text{and } (g-1) = floor(G.e_C) \tag{77}$$

It is because the carriers are distributed in uniform bandwidths that power and power factor versus control signal characteristics are the same as in the previous case. The novelty is that the power characteristic is defined by one and only one carrier depending on the value of e_c. This is an advantage which facilitates the search of the conditions to correct the non-linearity of power characteristic.

6.3. Third coordination: distribution in non-uniform bandwidths

Using Eqs. (74) and (76), we determine the slope of the power characteristic

$$\frac{dp}{de_C} = \frac{g^2 - (g-1)^2}{\widehat{Car}_g} \tag{78}$$

To linearize this power characteristic, all segments of the power characteristic must have the same slope G^2 (because, when e_C varies from 0 to 1, power varies from 0 to G^2):

$$\frac{dp}{de_C} = \frac{g^2 - (g-1)^2}{\widehat{Car}_g} = G^2 \tag{79}$$

It is thus deduced that to linearize the power characteristic, it is necessary that:

$$\widehat{Car}_g = \frac{g^2 - (g-1)^2}{G^2} \tag{80}$$

The carriers are therefore distributed in non-uniform bandwidths defined by:

$$\left(BL_{g-1} = \sum_{j=1}^{g-1} \widehat{Car}_j\right) \le e_C \le \left(BL_g = \sum_{j=1}^{g} \widehat{Car}_j\right) \tag{81}$$

Taking account of Eq. (80), the lower and upper limits of a bandwidth become:

$$\begin{cases} BL_{g-1} = \sum_{j=1}^{g-1} \widehat{Car}_j = (g-1)^2/G^2 \\ BL_g = \sum_{j=1}^{g} \widehat{Car}_j = g^2/G^2 \end{cases} \tag{82}$$

For example, if one considers an MPDMC with three inverters, the three carriers and the three bandwidths are (**Figure 15**):

Car_1 : covers [0 1/9], its pic-value is $\widehat{Car}_1 = 1/9$ and its upper limit: $B_1 = 1/9$

Car_2 : covers [1/9 4/9], its pic-value is $\widehat{Car}_2 = 3/9$ and its upper limit: $B_2 = 4/9$

Car_3 : covers [4/9 9/9], its pic-value is $\widehat{Car}_3 = 5/9$ and its upper limit: $B_3 = 9/9$

The pattern duty cycle is defined by:

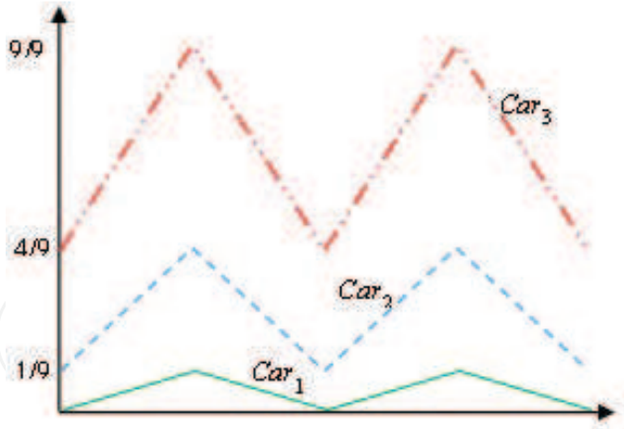


Figure 15. Carriers distributed in non-uniform bandwidths, $G=3$.

$$d = \frac{e_c - BL_{g-1}}{BL_g - BL_{g-1}} \text{ if } BL_{g-1} \le e_c \le BL_g \tag{83}$$

Substitution of Eq. (82) into Eq. (83) yields:

$$d = \frac{G^2 e_c - (g-1)^2}{2g-1} \text{ with } (g-1) = floor(G\sqrt{e_c}) \tag{84}$$

Substitution of Eq. (84) into Eq. (74) leads to the expression of transmitted power:

$$p = G^2 e_c \tag{85}$$

Substitution of Eq. (84) into Eq. (75) leads to the expression of transmitted power:

$$PF = \frac{G^2 e_c}{\sqrt{G^2 e_c \left(g^2 + (g-1)^2\right) - g^2 (g-1)^2}} \text{ with } (g-1) = floor(G\sqrt{e_c}) \tag{86}$$

Eqs. (85) and (86) show that the power characteristic is linear and that the power factor is unitary in G points:

$$PF = 1 \text{ when } e_c = BL_g = (g/G)^2 \text{ or when } p = g^2 \text{ with } g = 1, 2, \ldots G \tag{87}$$

7. Simulation results

Simulations are carried out in the Matlab SimPowerSystems environment. We consider a RLC load (1.85 Ω, 20 μH, 90 nF), matching transformer ration 3/10 and an ac-supply 120 V-60 Hz. The results of four simulation series are presented. **Figures 16** and **17** show examples of currents drawn by a PDMC and $MPDMC_2$. **Figures 18** and **19** show the theoretical and simulation results of transmitted power and power factor characteristics in the case of PDMC. **Figures 20** and **21** show the theoretical and simulation results of transmitted power and power factor characteristics in the case of $MPDMC_2$ and coordination's types 1, 2 and 3. We note a good agreement between theoretical and simulation results.

http://dx.doi.org/10.5772/intechopen.68324

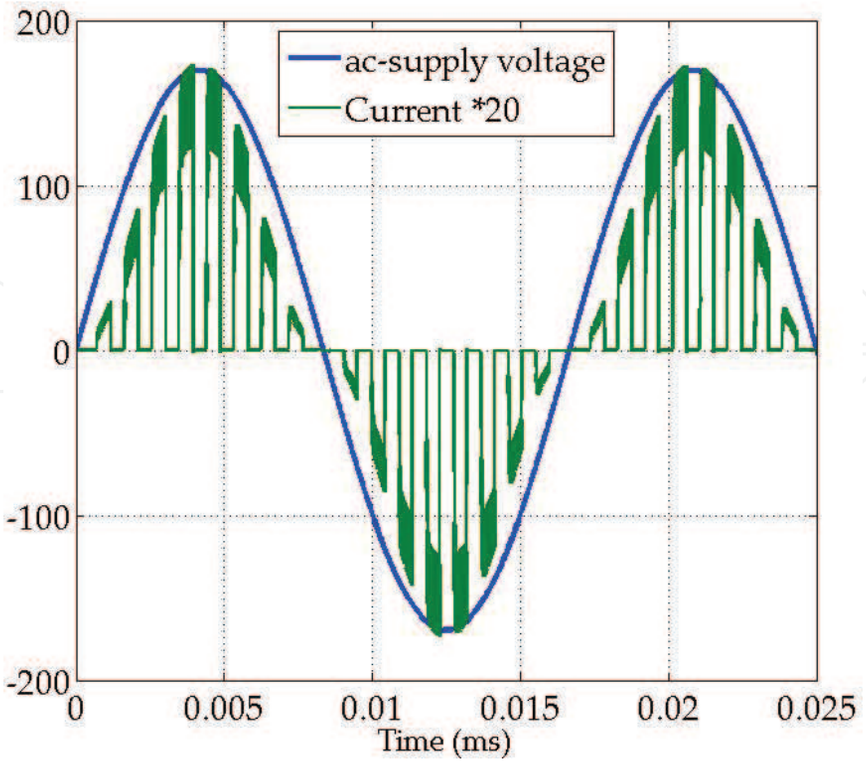


Figure 16. Current drawn by PDMC, $e_c = 0.5$.

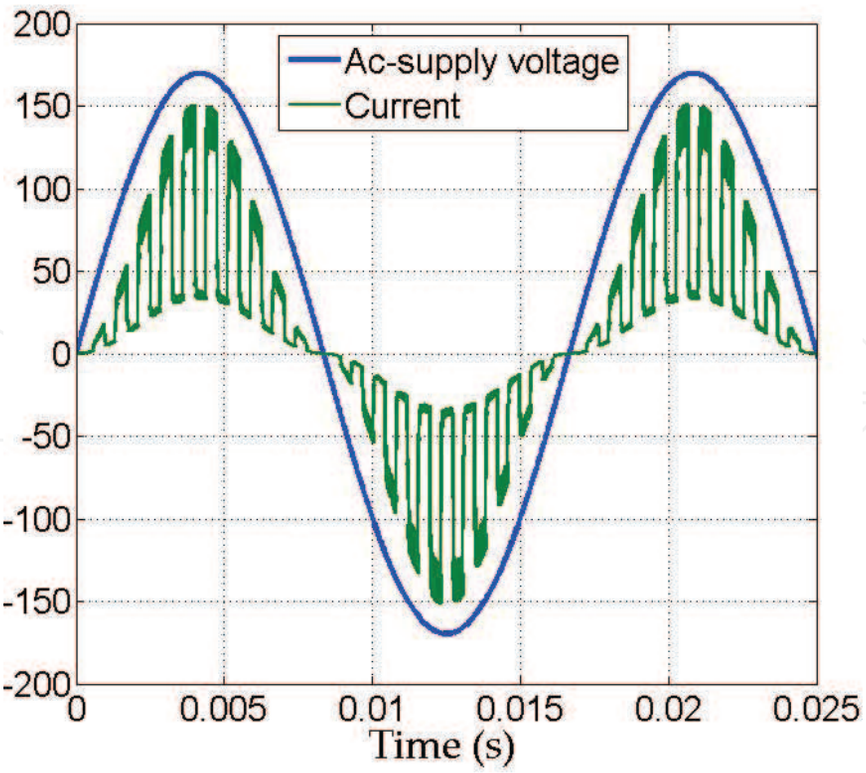


Figure 17. Current drawn by $MPDMC_2$ carriers coordination type 2, $e_c = 0.75$.

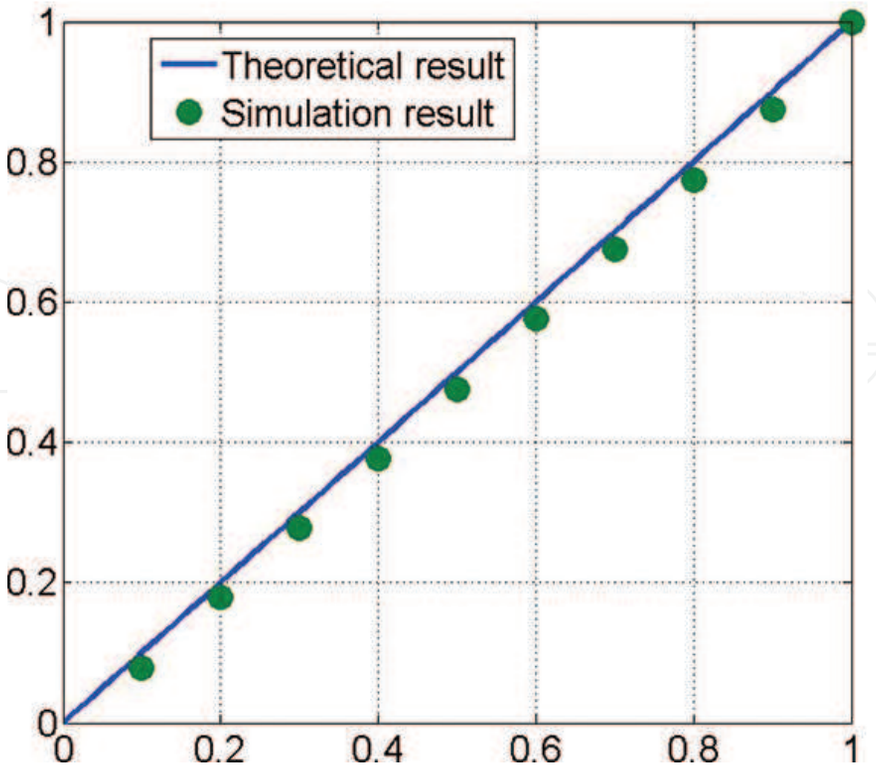


Figure 18. Power versus e_c characteristic of PDMC.

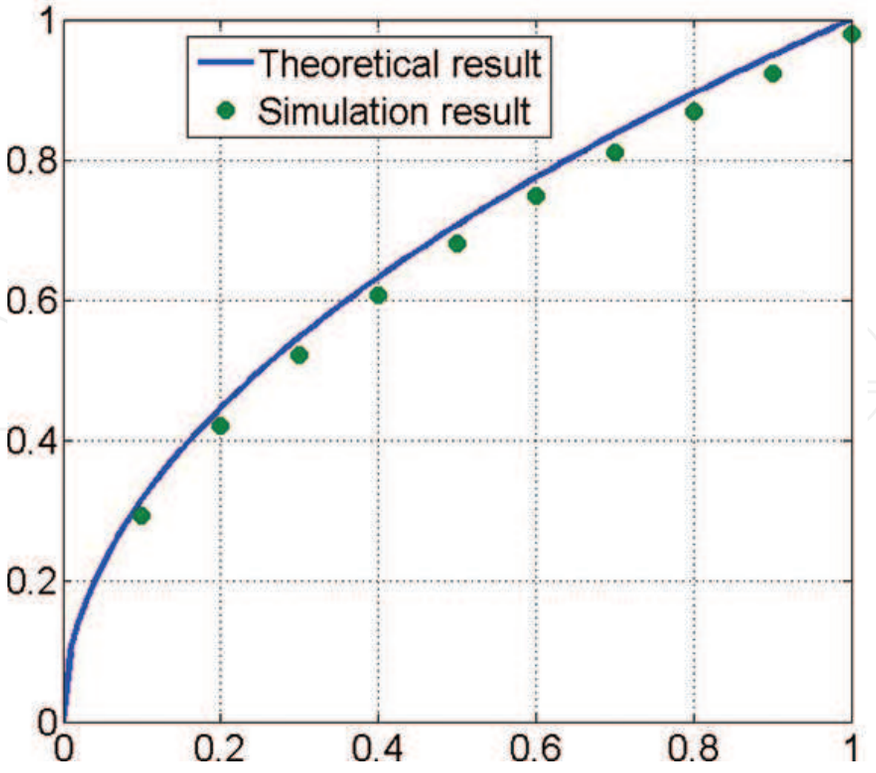


Figure 19. Power factor versus e_c characteristic of PDMC.

http://dx.doi.org/10.5772/intechopen.68324

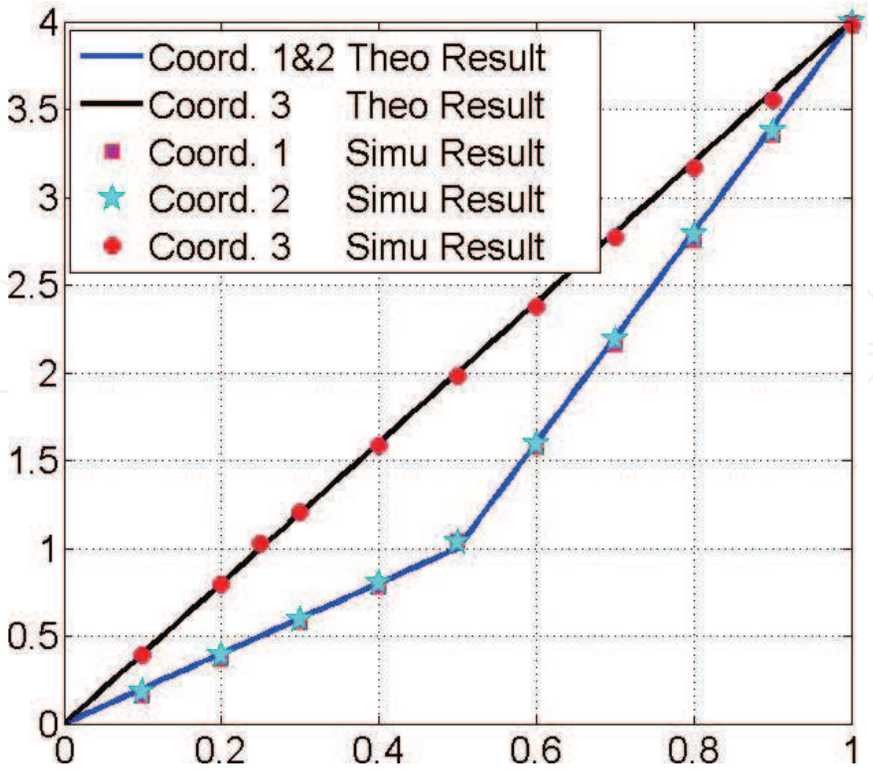


Figure 20. Power versus e_c characteristic of $MPDMC_2$.

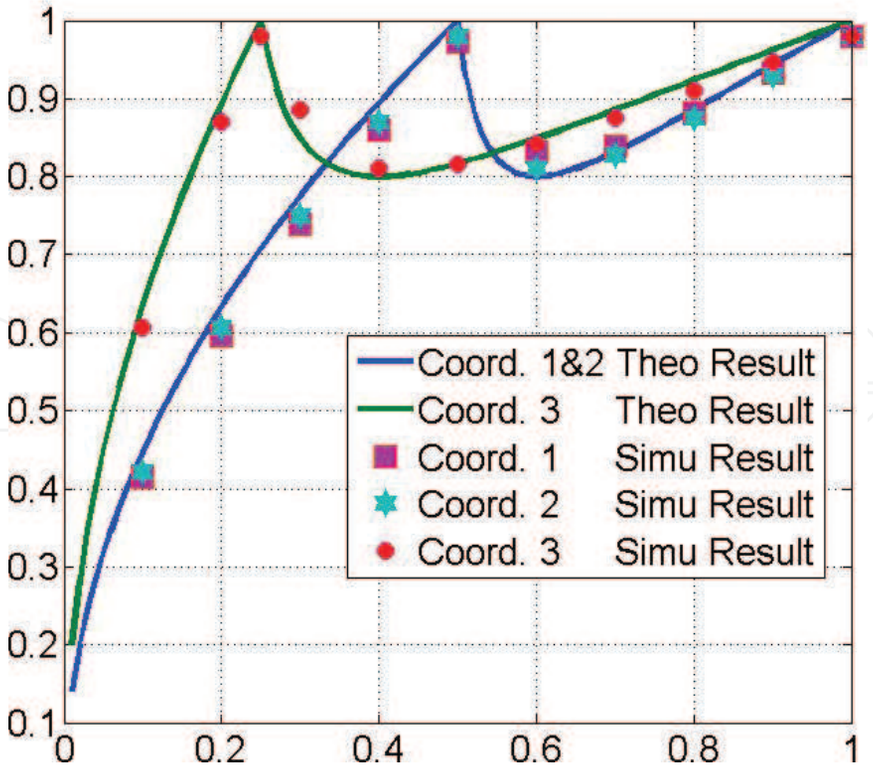


Figure 21. Power factor versus e_c characteristic of $MPDMC_2$.

8. Conclusion

The reflections and results presented in this chapter can be divided into two groups: the background and the novelties.

The background includes the PDM control principle, the PDM pattern generation and the characteristics of the ac-ac PDM converter and ac-ac Multi-PDM converter. In the description of the PDM control principle, we deliberately sought to present the PDM control as a form of association based on role sharing between the concepts of soft switching and hard switching. The role of soft switching is to produce lossless switching, while the role of hard switching is to vary the power by deciding the nature of the switching cycles. This reflection on the nature of the PDM control led us to represent the operation of the PDM inverter by a setting in cascade of a chopper and a series resonant inverter. We have detailed a PDM pattern generation method for the ac-ac PDM converter. It is a method inspired by PWM techniques, but adapted to the specificities of the PDM control (adaptation of the pattern frequency to both the resonant frequency and the ac-supply frequency). This method is based on a synchronous comparison of a carrier with a control signal and a calibration of the useful period of the dc voltage. Without the detailed, we have given the power transmitted characteristics and the spectrum of the current drawn from the ac-supply by an ac-ac PDM converter. Without detailed, we gave the characteristics of the transmitted power and the spectrum of the current drawn from the electrical communication by a ac-ac PDM converter. The power-factor correction by a total or partial mutual compensation is presented. It leads to the definition of a converter with several inverters and interlaced carriers. This is the ac-ac multi-PDM converter. The behavior of this converter is modeled by a system bi-converter.

The novelties include mainly the average modeling of ac-ac PDM converter and ac-ac multi-PDM converter and the introduction of carrier coordination as a control parameter of ac-ac multi-PDM converter. The application of average modeling leads to the representation of the series resonant inverter by an equivalent RL branch. The replacement of the inverter by its equivalent RL branch in the ac-ac PDM converter facilitates the analysis of this converter and makes it possible to establish (i) the conditions to preserve the linearity of the power characteristic and (ii) an analytical expression of the power-factor. The replacement of the inverter by its equivalent RL branch in the ac-ac Multi-PDM converter allows modeling this converter by an operating model (a model that integrates the operations of the components of the converter). This makes it possible to envisage several types of coordination. Three types of coordination are presented. Coordination by stratified carriers allows (i) a power-factor correction based on the search for a minimal distortion (ii) and to linearize the power characteristic.

Appendix

By subdividing $[0\ \pi]$ into q PDM pattern periods, the expressions of the fundamental component and the RMS-value of the drawn current are written:

$$\hat{I}_{ac,f} = \frac{2}{\pi}\sum_{j=1}^{q}\int_{(j-1)\pi/q}^{j\pi/q} i_{dc} sin(\theta) d\theta \tag{A.1}$$

$$I_{ac}{}^2 = \frac{2}{\pi}\sum_{j=1}^{q}\int_{(j-1)\pi/q}^{j\pi/q} i_{dc}{}^2 d\theta \tag{A.2}$$

Assuming that q is large enough so that the *sin* varies very little over the interval $[(j-1)\pi/q\ j\pi/q]$, we write that:

$$sin(\theta) = sin\Big(\theta_j = (\pi/q)(j-1/2)\Big) \tag{A.3}$$

Taking into account Eqs. (A.3) and (A.1) becomes:

$$\hat{I}_{ac,f} = \frac{2}{\pi}\sum_{j=1}^{q} sin(\theta_j)\int_{(j-1)\pi/q}^{j\pi/q} i_{dc} d\theta \tag{A.4}$$

Knowing that average and RMS values of i_{dc} are as follows:

$$\langle i_{dc}\rangle(j) = \frac{\pi}{q}\int_{(j-1)\pi/q}^{j\pi/q} i_{dc} d\theta \tag{A.5}$$

$$\boldsymbol{I_{dc}(j)^2 = \frac{q}{\pi}\int_{(j-1)\pi/q}^{j\pi/q} i_{dc}{}^2 d\theta} \tag{A.6}$$

It is established that:

$$\hat{I}_{ac,f} = \frac{2}{q}\sum_{j=1}^{q} sin(\theta_j)\langle i_{dc}\rangle(j) \tag{A.7}$$

$$\boldsymbol{I_{ac}{}^2 = \frac{1}{\pi}\sum_{j=1}^{q}\frac{\pi}{q} I_{dc}(j)^2} \tag{A.8}$$

Substitutions of Eq. (32) into Eqs. (A.7) and (37) into Eq. (A.8) yield:

$$\hat{I}_{ac,f} = \frac{\hat{V}_{ac}}{R_{eq}}\left\{d - \frac{\tau_{eq}}{T_{PDM}}\frac{\left(1-exp\left(-d\frac{T_{PDM}}{\tau_{eq}}\right)\right)\left(1-exp\left(-(1-d)\frac{T_{PDM}}{\tau_{eq}}\right)\right)}{1-exp\left(-\frac{T_{PDM}}{\tau_{eq}}\right)}\right\}\frac{2}{q}\sum_{j=1}^{q} sin(\theta_j)^2 \tag{A.9}$$

$$\frac{I_{ac}{}^2}{\left(\frac{\hat{V}_{ac}}{R_{eq}}\right)^2} = \left\{d - \frac{2\tau_{eq}}{T_{PDM}}\frac{1-e^{-(1-d)\frac{T_{PDM}}{\tau_{eq}}}}{1-e^{-\frac{T_{PDM}}{\tau_{eq}}}}\left\{1 - e^{-d\frac{T_{PDM}}{\tau_{eq}}} + \frac{\left(1-e^{-(1-d)\frac{T_{PDM}}{\tau_{eq}}}\right)\left(1-e^{-2d\frac{T_{PDM}}{\tau_{eq}}}\right)}{4\left(1-e^{-\frac{T_{PDM}}{\tau_{eq}}}\right)}\right\}\right\}\frac{\sum_{j=1}^{q} sin(\theta_j)^2}{q} \tag{A.10}$$

Knowing that:

$$\sum_{j=1}^{q} sin(\theta_j)^2 = q/2 \tag{A.11}$$

Eqs. (A.9) and (A.10) becomes:

$$\hat{I}_{ac,f} = \frac{\hat{V}_{ac}}{R_{eq}}\left\{d - \frac{\tau_{eq}}{T_{PDM}}\left(1 - exp\left(-d\frac{T_{PDM}}{\tau_{eq}}\right)\right)\left(1 - exp\left(-(1-d)\frac{T_{PDM}}{\tau_{eq}}\right)\right)/1 - exp\left(-\frac{T_{PDM}}{\tau_{eq}}\right)\right\} \tag{A.12}$$

$$I_{ac}{}^2 = \frac{\hat{V}_{ac}{}^2}{2R_{eq}{}^2}\left\{d - \frac{2\tau_{eq}}{T_{PDM}}\frac{1 - e^{-(1-d)\frac{T_{PDM}}{\tau_{eq}}}}{1 - e^{-\frac{T_{PDM}}{\tau_{eq}}}}\left\{1 - e^{-d\frac{T_{PDM}}{\tau_{eq}}} + \frac{\left(1 - exp\left(-d\frac{T_{PDM}}{\tau_{eq}}\right)\right)\left(1 - exp\left(-(1-d)\frac{T_{PDM}}{\tau_{eq}}\right)\right)}{4\left(1 - exp\left(-\frac{T_{PDM}}{\tau_{eq}}\right)\right)}\right\}\right\} \tag{A.13}$$

Taking into account Eqs. (32) and (33), we obtain:

$$\hat{\boldsymbol{I}}_{\boldsymbol{ac,f}} = \langle \boldsymbol{i}_{\boldsymbol{dc}} \rangle_{\boldsymbol{T_{PDM}}}(\boldsymbol{j})/\boldsymbol{sin}(\boldsymbol{\theta}_j) \tag{A.14}$$

$$\boldsymbol{I}_{\boldsymbol{ac}} = \boldsymbol{I}_{\boldsymbol{dc}}(\boldsymbol{j})/\sqrt{\boldsymbol{2}}\boldsymbol{sin}(\boldsymbol{\theta}_j) \tag{A.15}$$

Nomenclature

$A\left(=exp(-\alpha T_r/2)\right)$	Intermediate constant
C	Load's capacitor
F_{ac} (T_{ac})	Ac-supply frequency (period)
L	Load's inductor
R	Load's resistor
T_{dc} $(=T_{ac}/2)$	Period of voltage rectified
T_{PDM}	PDM pattern
T_r	Resonance period
$\hat{V_{ac}}$	Amplitude of ac-supply voltage
d	Duty cycle of PDM pattern
$floor$	Integer portion
k	PDM pattern length
q	PDM pattern frequency in pu $(F_{PDM} = q2F_{ac})$
$\alpha(=R/2L)$	Attenuation factor
$\tau_{eq}(=L_{eq}/R_{eq})$	Time constant of RL equivalent branch
$\xi\left(=(R/2)\sqrt{C/L}\right)$	Damping ratio

Author details

Abdelhalim Sandali[1]* and Ahmed Chériti[2]

*Address all correspondence to: sandali@uqtr.ca

1 University Hassan II Casablanca - ENSEM, Casablanca, Morocco

2 University of Quebec at Trois-Rivières, Trois-Rivières, Quebec, Canada

References

[1] Divan DM, Venkataramanan G, De Doncker RW. Design methodologies for soft switched inverters. In: IEEE, editor. IAS Annual meeting; October 2–7; Pittsburgh. Pennsylvania: IEEE; 1988. pp. 758–766. DOI: 10.1109/IAS.1988.25147

[2] Liu KH, Oruganti R, Lee FC. Quasi-resonant converters topologies and characteristics. IEEE-Transactions on Power Electronics. 1987;**PE-2**(1):62–71. DOI: 10.1109/TPEL.1987.4766333

[3] Li R, Xu D. A zero-voltage switching three-phase inverter. IEEE Transactions on Power Electronics. 2014;**29**(3):1200–1210. DOI: 10.1109/TPEL.2013.2260871

[4] Outeiro MT, Buja G, Czarkowski D. Resonant power converters: an overview with multiple elements in the resonant tank network. IEEE Industrial Electronics Magazine. 2016;**10**(2):21–45. DOI: 10.1109/MIE.2016.2549981

[5] Enhui Chu, Xing Zhang, Liang Huang. Research on a novel modulation strategy fot double auxiliary resonant commuted pole soft-switching inverter with the shunt dead time. IEEE Transactions on Power Electronics. 2016;**31**(10):6855–6869. DOI: 10.1109/TPEL.2015.2508143

[6] Fujita H, Akagi H. Pulse density modulated power control of a 4 kW, 450 kHz voltage-source inverter for induction melting applications. IEEE Transactions on Industry Applications. 1996;**32**(2):279–286. DOI: 10.1109/28.491475

[7] Fujita H, Akagi H. Control and performance of a pulse density modulated series-resonant inverter for corona discharge processes. IEEE Transactions on Industry Applications. 1999;**35**(3):621–227. DOI: 10.1109/28.767013

[8] Esteve V, Jordán J, Sanchis-Kilders E, Dede Enrique J, Maset E, Ejea Juan B, Ferreres A. Enhanced pulse-density-modulated power control for high-frequency induction heating inverters. IEEE Transactions on Industry Electronics. 2015;**62**(11):6905–6914. DOI: 10.1109/TIE.2015.2436352

[9] Lucia O, Sarnago H, Burdio JM. Pulse density modulated control for the series resonant multi-inverter for induction heating applications. In: IEEE, editor. IECON—42nd Annual

Conference of the IEEE Industrial Electronics Society; October 24–27; Firenze (Florence), Italy: 2016. pp. 5995–6000. DOI: 10.1109/IECON.2016.7794026

[10] Mousavian H, Abnavi S, Bakhshai A, Jain P. A push-pull Class E converter with improved PDM control. In: IEEE, editor. 7th International Symposium on Power Electronics for Distributed Generation Systems (PEDG); 27–30 June; Vancouver, Canada. Vancouver, Canada: IEEE; 2016. DOI: 10.1109/PEDG.2016.7527053

[11] Mishima T, Nakaoka M. A load-power adaptive dual pulse modulated current phasor-controlled ZVS high-frequency resonant inverter for induction heating applications. IEEE Transactions on Power Electronics. 2014;**29**(8):3864–3880. DOI: 10.1109/TIE.2013.2288985

[12] Sandali A, Cheriti A, Sicard P. Design considerations for PDM Ac-ac converter implementation. In: IEEE, editor. Annual IEEE Applied Power Electronics Conference and Exposition (APEC'07); February 25–March 1; Anaheim, California: IEEE; 2007. pp. 1678–1683. DOI: 10.1109/APEX.2007.357744

[13] Sandali A, Cheriti A, Sicard P, Al Haddad K. Application of PDM control to a multilevel ac-ac converter with self power factor correction. In: IEEE, editor. 35th Annual Power Electronics Specialists Conference (PESC'04); June 20–25; Aachen, Germany: IEEE; 2004. pp. 2881–2887. DOI: 10.1109/PESC.2004.1355291

[14] Lin W, Jovcic D. Average modelling of medium frequency DC-DC converters in dynamic studies. IEEE Transactions on Power Delivery. 2015;**30**(1):281–289. DOI: 10.1109/TPWRD.2014.2321425

[15] Xiao Liu, Aaron M. Cramer, Fei Pan. Generalized average method for time-invaring modeling of inverters. IEEE Transactions on Circuits and Systems. 2017;**64**(3):740–751. DOI: 10.1109/TCSI.2016.2620442

[16] Sandali A, Cheriti A. Accurate average model of PDM dual inverter. International Review on Modelling and Simulations. 2014;**7**(5):816–828. DOI: ISSN-19749821

IntechOpen